

A General Tensor Prediction Framework Based on Graph Neural Networks

Yang Zhong,^{II} Hongyu Yu,^{II} Xingao Gong, and Hongjun Xiang*



Cite This: *J. Phys. Chem. Lett.* 2023, 14, 6339–6348



Read Online

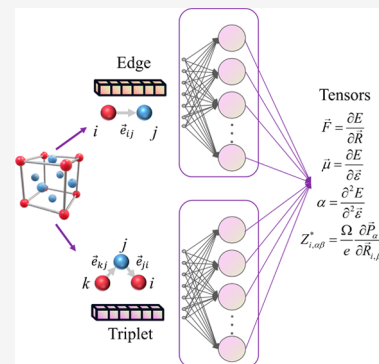
ACCESS |

Metrics & More

Article Recommendations

Supporting Information

ABSTRACT: Graph neural networks (GNNs) have been shown to be extremely flexible and accurate in predicting the physical properties of molecules and crystals. However, traditional invariant GNNs are not compatible with directional properties, which currently limits their usage to the prediction of only invariant scalar properties. To address this issue, here we propose a general framework, i.e., an edge-based tensor prediction graph neural network, in which a tensor is expressed as the linear combination of the local spatial components projected on the edge directions of clusters with varying sizes. This tensor decomposition is rotationally equivariant and exactly satisfies the symmetry of the local structures. The accuracy and universality of our new framework are demonstrated by the successful prediction of various tensor properties from first to third order. The framework proposed in this work will enable GNNs to step into the broad field of prediction of directional properties.



The development of machine learning (ML) is changing the traditional research paradigm of molecular and material science.^{1–3} Without performing the computationally demanding electronic structure calculations, ML can build an end-to-end mapping from structure to properties on the basis of the large databases to accelerate the development of materials.^{4–12} In addition, machine learning atomic potential with quantum-mechanical precision has been widely used to replace the costly first-principles calculations.^{13–16} The successful applications of ML in computational material science occurred largely because the adopted framework conforms to the fundamental symmetries of the system. As in the case of the traditional graph neural networks (GNNs)^{17–22} and classical kernel-based machine learning methods,^{23–26} the translational and rotational invariant features of the scalar properties are exploited to increase the accuracy and transferability for the prediction of scalar properties.

In addition to invariant scalar properties, various tensorial properties of materials are also important to the functions of materials. The tensorial properties of materials describe the response susceptibilities of materials to various external fields. For example, the dielectric tensor describes the response of an insulator to an electric field. The piezoelectric tensors describe the anisotropic response of materials to mechanical perturbations. The prediction of tensorial properties requires the models to be rotationally equivariant when the reference coordinate system is rotated. Most of the recently proposed equivariant networks are based on SO(3) representations to incorporate directional information.^{27–30} Because these conceptually complex networks use inconvenient Clebsch–

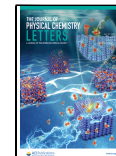
Gordon (CG) transforms on spherical harmonic bases to achieve equivariance, the conversion between one-dimensional SO(3) equivariant features and higher-order geometric tensors is not straightforward. So far, these networks have been reported to achieve very high accuracy in scalar prediction tasks but have rarely been used to predict the tensor properties of molecules and crystals.^{30–32}

In molecular and materials science, Gaussian process regression (GPR) based on an equivariant kernel is the earliest network architecture for tensor prediction. Grisafi et al. proposed a GPR equivariant model based on the symmetry-adapted smooth overlap of atomic positions (SOAP) kernels to predict the tensorial properties.³³ In this GPR framework, the geometric tensors are decomposed into a series of irreducible spherical tensor (IST) representations that can be learned independently. The kernel methods based on IST decomposition rely on the construction of fixed equivariant kernels to predict tensors. Hence, its accuracy and multielement generalization ability may be limited. Because the more flexible GNNs can learn a representation in a self-adaptive way and a single GNN can simultaneously deal with all elements in the whole periodic table, it is expected that GNNs would predict tensors more accurately than the usual descriptor-based ML approaches, similar to the case of predicting scalar properties.

Received: May 4, 2023

Accepted: July 3, 2023

Published: July 7, 2023



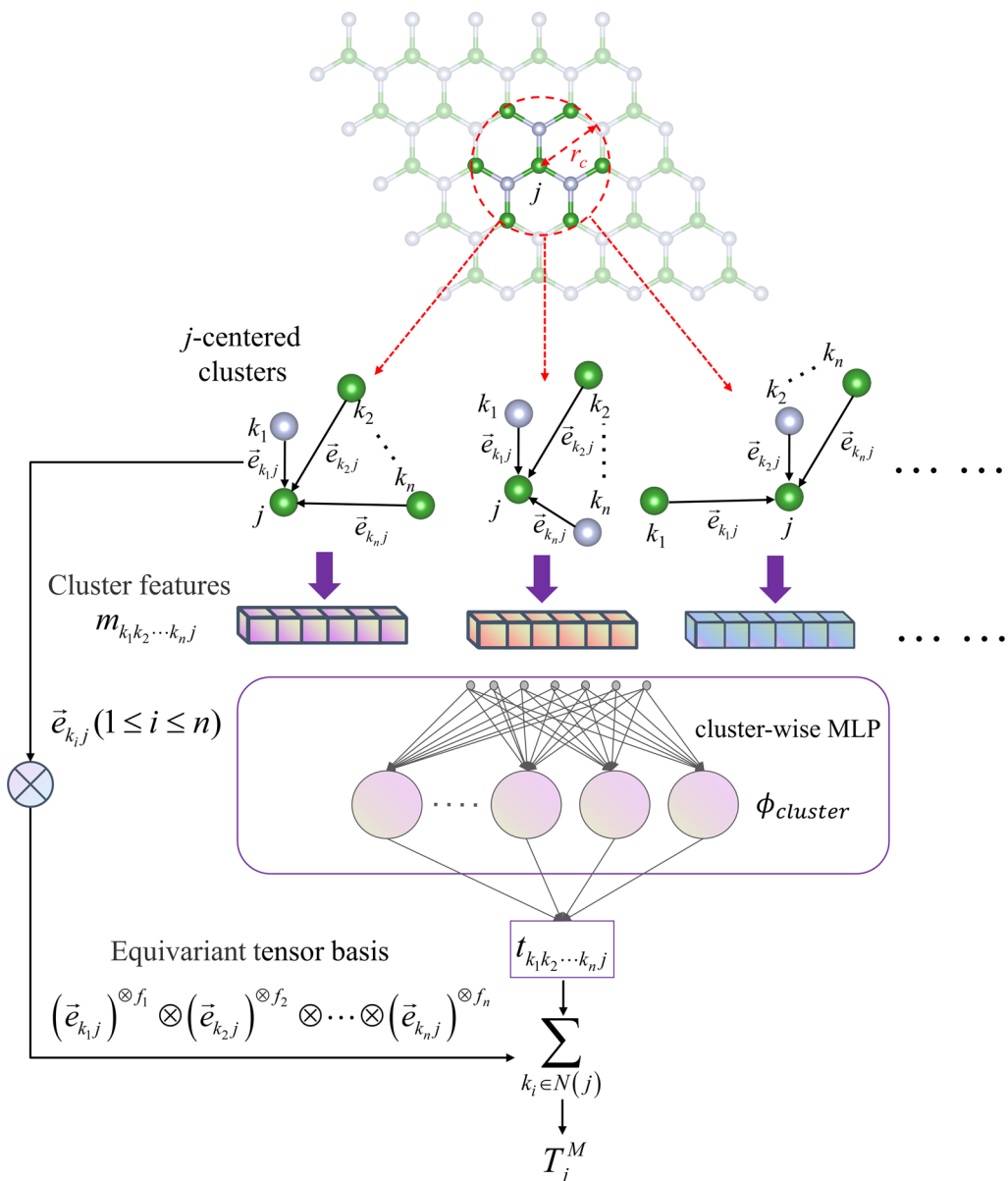


Figure 1. Schematic diagram of predicting the atomic rank- M tensors. The atomic rank- M tensors are expanded with the rank- M tensor bases constructed by M edge vectors, which contain n ($n \leq M$) individual neighbor atoms within a cutoff radius r_c . For symmetric tensor bases, the required number of individual neighbor atoms n can be less than M by using multifold tensor products of the edge vectors. The n individual neighbor atoms together with the central atom j form a cluster containing $n + 1$ atoms. The lengths of the edges and the angles between the edges in the cluster can be aggregated into the feature vector $m_{k_1 k_2 \dots k_n j}$ that can be updated iteratively. The corresponding tensor expansion coefficients $t_{k_1 k_2 \dots k_n j}$ are mapped from the features of each cluster through a clusterwise regression layer $\phi_{cluster}$. The tensor of atom j is obtained by summing the tensor contributions of each j -centered cluster.

Unfortunately, the usual invariant GNNs cannot be straightforwardly adopted to predict the equivariant tensor properties. Some modified GNNs for tensor prediction have been reported recently. Glick et al. proposed a Cartesian message-passing neural network (CMPNN) by introducing directional edge features between adjacent atoms to encode the Cartesian information.³⁴ This model successfully predicted atomic multipole moments. However, the message functions and update functions of this architecture have the same form as their invariant counterparts. Although this model adopted the data augmentation technique, the equivariance of the tensors is not strictly satisfied. Clearly, a general GNN-based framework for accurately predicting tensors is highly desirable. Zaverkin et

al. proposed an equivariant model called Gaussian-moment neural networks (GMNNs) to predict molecular tensors.³⁵ However, GMNNs have been applied to only the learning of the magnetic anisotropy tensors and may not be applied to the prediction of tensors with arbitrary orders. Recently, Nguyen et al.³⁶ decomposed each IST component that makes up the target property as a sum of each atomic tensor, which is represented by a local atomic environment descriptor defined by a linear combination of spherical harmonics. Their framework can use either linear regression or neural networks to predict the scalar coefficients before each local equivariant descriptor. On the basis of a similar local tensor expansion, we construct the local Cartesian tensor bases by using the

directional information on edges in graph-structured data. This transforms the prediction of equivariant tensors to the prediction of invariant scalar coefficients.

In this Letter, we propose a tensor prediction framework based on GNNs. The main idea of this framework is that the tensor property of a crystal can be represented as the average of the tensor contributions of all of the atoms in the crystal and that the tensor contribution of each atom can be expressed as the linear combination of the local spatial components projected on the edge directions of clusters with varying sizes. This framework can describe the general tensors of different orders and symmetries. To implement this framework, we designed an edge-based tensor prediction graph neural network (ETGNN) and tested its tensor prediction ability for a wide range of tensors, including the forces (\vec{F}), dipole moments (μ), polarizabilities (α), chemical shifts (σ), Born effective charges (BECs), and dielectric (DL), and piezoelectric (PZ) tensors. This approach is conceptually simple and enables various GNNs to predict tensors without making significant changes to the existing networks.

The equivariance of a tensor refers to the behavior that the tensor changes mathematically under the transformation of the coordination system, in contrast to the invariance of the scalar (e.g., the energy), which remains unchanged. The traditional GNNs embed the scalar information on graphs such as species and interatomic distance into the invariant features of nodes and edges, which are updated iteratively. GNNs in molecular and materials science widely adopt the atom-centric scalar prediction framework,³⁷ which expresses the energy of a crystal as the sum of the atomic energies predicted by the invariant features of atoms. Here, we generalize the atom-centric framework of GNNs to tensors and represent each crystal rank- M tensor property (T^M) as the average of the atomic rank- M tensor contributions (T_j^M). The key to the problem is how to predict atomic tensors. The illustration of predicting the atomic rank- M tensors in this framework is shown in Figure 1. This tensor prediction framework can be expressed by the following formulas:

$$T^M = \frac{1}{N} \sum_{j=1}^N T_j^M \quad (1)$$

$$T_j^M = \sum_{k_i \in N(j)} t_{k_1 k_2 \dots k_n} (\vec{e}_{k_j})^{\otimes f_1} \otimes (\vec{e}_{k_j})^{\otimes f_2} \otimes \dots \otimes (\vec{e}_{k_j})^{\otimes f_n} \quad (2)$$

where N is the number of atoms in the cell and \vec{e}_{k_j} is the unit edge vector from neighboring atom k_j to central atom j . $N(j)$ represents the set of all neighbor atoms of atom j within cutoff radius r_c . $(\vec{e}_{k_j})^{\otimes f_i}$ is the f_i -fold ($f_i \geq 1$) tensor product of \vec{e}_{k_j} , and $\sum_{i=1}^n f_i = M$. $t_{k_1 k_2 \dots k_n}$ is a scalar coefficient of the cluster containing n individual neighboring atoms, which can be derived from features $m_{k_1 k_2 \dots k_n}$ of the j -centered cluster. The summation in eq 2 runs over all of the permutations of n neighbors of atom j . Equation 2 is a general expression of the atomic rank- M tensor expansion, which requires at most M individual edge vectors to construct the tensor bases. For symmetric crystal tensors, we can represent it as the average of the symmetric atomic tensors that can be expanded with the symmetric tensor bases. In this case, n can be smaller than M because the symmetric tensor bases can be constructed by the multifold tensor product of the edge vectors. This can greatly

reduce the complexity of the formulas and the amount of unnecessary calculations.

One can easily show that the tensors predicted by ETGNN strictly satisfy the equivariance condition. The tensor product of two vectors $u^{(l_1)}$ and $v^{(l_2)}$ of orders l_1 and l_2 is a prescription for obtaining another equivariant vector or tensor $(u \otimes v)^{(l_1 \otimes l_2)}$ in higher-order vector space. Because each edge vector in real space is rotationally equivariant, the tensors obtained by the tensor product of multiple edge vectors are also equivariant. In addition, the atomic tensor constructed by eq 2 satisfies the proper symmetry of the local structure as all of the neighboring atoms [$k_i \in N(j)$] of a central atom (i.e., the j th atom here) are considered in the summation. If the cluster centered on atom j is symmetric with respect to the rotation or inversion operation R around atom j [i.e., $\forall k_i \in N(j)$, $R\vec{r}_{k_i} = \vec{r}_{k'_i}$, where $k'_i \in N(j)$], then the summation in eq 2 remains unchanged. It is a huge advantage that the atomic tensor expansion satisfies the symmetry of the atomic local structures inherently without learning the symmetry of the local structure through data augmentation or redundant network parameters. We also checked that the tensors predicted by our ETGNN model are indeed compatible with the symmetry of the examined system (see [Supplementary Discussion 1 in the Supporting Information](#) for details). Note that the equivariant tensors constructed by eqs 1 and 2 apply to all periodic and nonperiodic systems.

Below we will describe the details of the expansion of the tensors with respect to the edge directions taking force vector, BEC, DL, and PZ tensors as examples. The force vector and BEC of each atom can be directly represented by the corresponding atomic tensor contribution T_j^M , while the dipole moment, DL, and PZ tensors describing the whole crystal are represented by the average of the tensor contributions T_j^M of each atom in the primitive cell.

The force on the j th atom is the sum of the forces from the surrounding neighbor atoms:

$$\vec{F}_j = \sum_{k \in N(j)} t_{kj} \vec{e}_{kj} \quad (3)$$

The coefficients t_{kj} are the magnitudes of the forces between the atoms.

Because BEC is an asymmetric second-order tensor, the terms in eq 2 are explicitly split into the symmetric part T_j^{sym} and the nonsymmetric part T_j^{nonsym} :

$$T_j = T_j^{\text{sym}} + T_j^{\text{nonsym}} \quad (4)$$

$$T_j^{\text{sym}} = \sum_{k \in N(j)} t_{kj} \vec{e}_{kj} \otimes \vec{e}_{kj} \quad (5)$$

$$T_j^{\text{nonsym}} = \sum_{\substack{k, i \in N(j) \\ k \neq i}} t_{kji} \vec{e}_{kj} \otimes \vec{e}_{ji} \quad (6)$$

T_j^{sym} is expanded with second-order symmetric tensor bases $\vec{e}_{kj} \otimes \vec{e}_{kj}$ constructed by unit direction vectors \vec{e}_{kj} between atom pairs kj . T_j^{nonsym} is expanded with asymmetric tensor bases $\vec{e}_{kj} \otimes \vec{e}_{ji}$ constructed by unit direction vectors \vec{e}_{kj} and \vec{e}_{ji} . Because T_j^{sym} and T_j^{nonsym} require one and two individual neighbor atoms, respectively, expansion coefficients t_{kj} and t_{kji} are mapped from the hidden features of the edge messages (m_{kj}) and the triplet messages (m_{kji}), respectively. The embedding and updating of the triplet messages (m_{kji}) are illustrated in

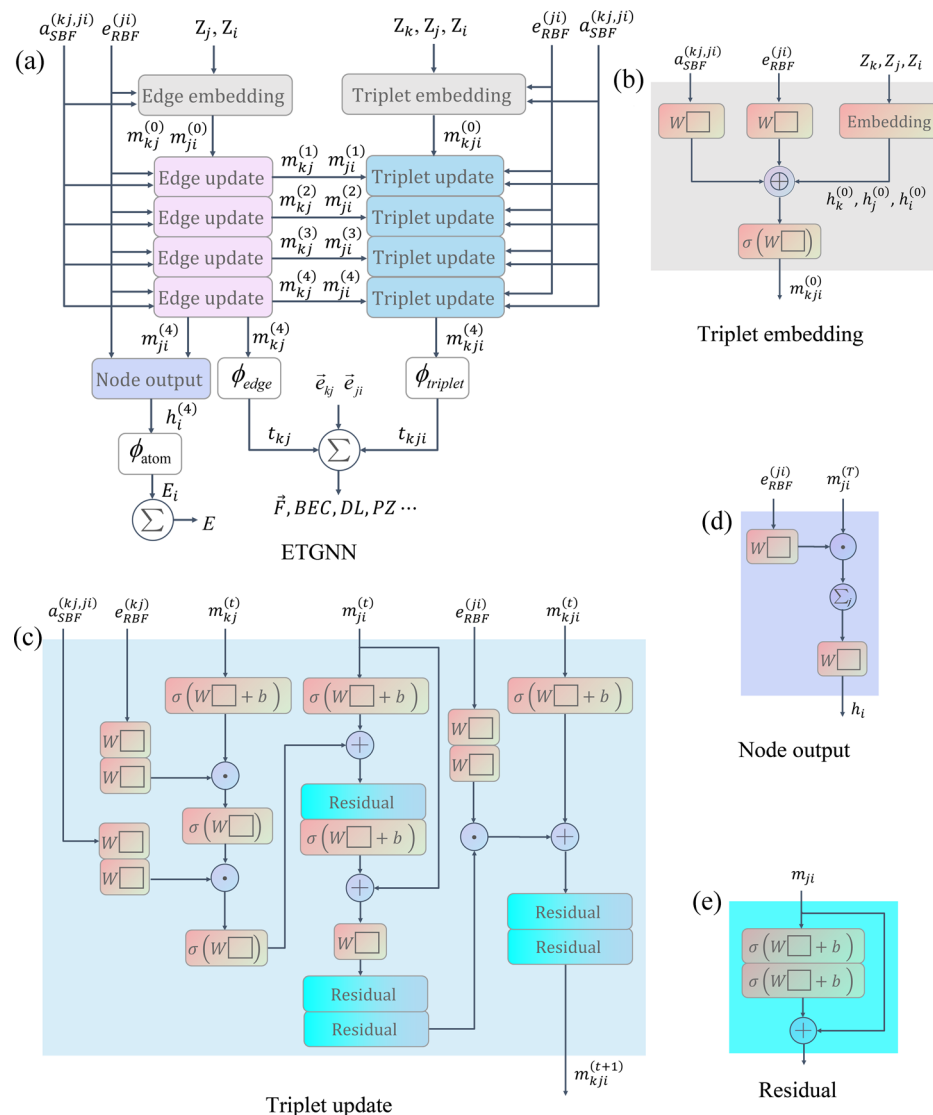


Figure 2. Architecture of ETGNN and its subnetworks. (a) Architecture of ETGNN with four layers of edge and triplet update blocks. The edge embedding and edge update blocks are inherited from the original embedding and interaction blocks of DimeNet++, so that the high precision of DimeNet++ can be retained. The initial features of the triplets are generated in (b) the triplet embedding block and are updated through (c) the triplet update blocks. The output of the last edge update block can be aggregated into the node features for scalar outputs by the (d) node output block. Panel e shows the residual block,²⁰ which is a multilayer feed-forward neural network with a short-cut connection to avoid the vanishing gradients problem.

detail below. It is important to note that the expansion formula of BEC can be applied to all second-order atomic tensors.

The DL tensor is a second-order symmetric tensor of the whole crystal and is not extended with the expansion of the primitive cell of the crystal. The DL tensors can be represented as the average of the atomic contributions of second-order symmetric tensors T_j^{sym} . Therefore, the edge-based expansion of the DL tensor can be written as

$$\text{DL} = \frac{1}{N} \sum_{j=1}^N \sum_{k \in N(j)} t_{kj} \vec{e}_{kj} \otimes \vec{e}_{kj} \quad (7)$$

The PZ tensor is a third-order symmetric tensor. According to the discussion presented above, the edge-based expansion formula of the PZ tensor is given as follows:

$$\text{PZ} = \frac{1}{N} \sum_{j=1}^N \left[\sum_{k \in N(j)} t_{kj} (\vec{e}_{kj})^{\otimes 3} + \sum_{\substack{k, i \in N(j) \\ k \neq i}} t_{kji} \vec{e}_{kj} \otimes (\vec{e}_{ji})^{\otimes 2} \right] \quad (8)$$

The first term is constructed by the 3-fold tensor product of \vec{e}_{kj} , and the second term is constructed by the tensor product of \vec{e}_{kj} with the 2-fold tensor product of \vec{e}_{ji} . Both terms satisfy the symmetry of $T_{abc} = T_{acb}$.

In traditional GNNs, the features of each atom are embedded in a high-dimensional space and are updated by passing messages between atoms. The contribution of each atom to the scalar property of a crystal is finally obtained through an atomwise regression neural network. According to the tensor prediction framework discussed above, the expansion coefficients of tensors up to an order of three are

mapped from the features of the edges or the triplets. In this work, we designed the edge-based tensor prediction graph neural network (ETGNN), which is a modified version of DimeNet++.³⁸ Although in principle any common GNN can be adopted to predict tensor properties within our framework, here we adopt DimeNet++ as it is an invariant GNN that was shown to be highly precise in the prediction of scalar properties.^{22,38} ETGNN obtains the tensor expansion coefficients by updating the learned embeddings of the edges and triplets in the crystal graphs.

ETGNN has inherited the directional message-passing framework used by DimeNet++; i.e., atom features h_j and h_i and edge features $u_{ij}^{(k)}$ of atom pairs ji are integrated into directional edge message $m_{ji}^{(k)}$ being sent from atom j to atom i , where k is the index of the multiplicity of the edges. Furthermore, ETGNN introduces an additional triplet component into the crystal graph, which is composed of node j and its two neighbor nodes, k and i . The nodes, edges, and angles contained in the triplets are embedded in triplet messages m_{kji} . Using equivariant expressions of tensors proposed in this work, ETGNN can predict both scalars and various tensor properties, such as forces \vec{F} , BECs, and DL and PZ tensors. ETGNN can realize the following mapping:

$$f_\theta: \{m_{kj}^{(k_1)}, \dots, m_{ji}^{(k_2)}, \dots, m_{kji}^{(k_1, k_2)}, \dots\} \rightarrow R, \vec{F}, \text{BEC}, \text{DL}, \text{PZ}, \dots \quad (9)$$

where θ is the learnable parameters of the network.

The architecture of the ETGNN is shown in Figure 2a. We kept the existing architecture in DimeNet++ and introduced the triplet embedding and the triplet update blocks. For tensor prediction, an edgewise layer ϕ_{edge} and a tripletwise layer ϕ_{triplet} are used to obtain the coefficients in the tensor expansion: $t_{kj} = \phi_{\text{edge}}(m_{kj})$, and $t_{kji} = \phi_{\text{triplet}}(m_{kji})$.

The triplet embedding block is shown in Figure 2b. The triplet message is embedded on the basis of distances $|\vec{r}_{kj}|$ and $|\vec{r}_{ji}|$ between node j and its neighbor nodes k and i , angle α_{kji} between \vec{r}_{kj} and \vec{r}_{ji} , and atomic numbers Z_k , Z_j , and Z_i . The spherical Bessel function $\phi_{\text{SBE}}: (R^1, R^1) \rightarrow R^{N_{\text{SRBF}} N_{\text{SHBF}}}$ is used as the two-dimensional joint bases of distances $|\vec{r}_{kj}|$ and angles α_{kji} in the triplets:

$$\phi_{\text{SBE}}(|\vec{r}_{kj}|, \alpha_{kji}) = \sqrt{\frac{2}{r_c^3 j_{l+1}^2(z_{ln})}} j_l \left(\frac{z_{ln}}{r_c} |\vec{r}_{kj}| \right) Y_l^0(\alpha_{kji}) \quad (10)$$

where j_l is the first kind of spherical Bessel function of order l and z_{ln} is its n th root ($0 \leq l \leq N_{\text{SHBF}} - 1$, and $1 \leq n \leq N_{\text{SRBF}}$). The expansion coefficients of the spherical Bessel function are multiplied by the cosine cutoff function to obtain the two-dimensional joint basis representation of $|\vec{r}_{kj}|$ and α_{kji} : $a_{\text{SBE}}^{(k_j, j)} = f_c(|\vec{r}_{kj}|) \phi_{\text{SBE}}(|\vec{r}_{kj}|, \alpha_{kji})$. Then the coefficients of the basis functions are linearly combined through a self-interaction layer $\varphi_{\text{SBE}}: R^{N_{\text{SRBF}} N_{\text{SHBF}}} \rightarrow R^{n_{\text{tri}}}$, where n_{tri} is the number of the hidden features of the triplets and equals 128 in this work. According to $a_{\text{SBE}}^{(k_j, j)}$, $e_{\text{RBF}}^{(ji)}$, and atomic numbers Z_k , Z_j , and Z_i , the embedding of the triplet can be constructed in the following formula:

$$m_{kji}^{(0)} = \sigma(W\{g(Z_i) \oplus g(Z_j) \oplus g(Z_k)\} \oplus \varphi_{\text{SBE}}[a_{\text{SBE}}^{(k_j, ji)}] \oplus \varphi_{\text{RBF}}[e_{\text{RBF}}^{(ji)}]) + b \quad (11)$$

where σ is ELU activation function³⁹ and g is a learnable atomic embedding layer.

The embeddings of edge messages and triplet messages are updated through multiple edge and triplet update blocks. The goal of ETGNN is to achieve the prediction of the tensor properties, so the edge update block adopts the original interaction layer in DimeNet++ to ensure that the modified network has the same accuracy as the original one. The triplet update block uses a directional message-passing mechanism similar to that in the edge update block. The update of the features of the triplets can be expressed by the following formula:

$$m_{kji}^{(t+1)} = f_{\text{update}}\{m_{kji}^{(t)}, f_{\text{int}}[m_{kj}^{(t)}, m_{ji}^{(t)}, e_{\text{RBF}}^{(kj)}, e_{\text{RBF}}^{(ji)}, a_{\text{SBE}}^{(kj, ji)}]\} \quad (12)$$

where f_{update} and f_{int} are the update function and interaction function, respectively, which are implemented by neural networks. The hidden features of triplets $m_{kji}^{(t)}$ are updated using directional edge messages $m_{kj}^{(t)}$ and $m_{ji}^{(t)}$ at the same layer. Angle α_{kji} between directional edge messages $m_{kj}^{(t)}$ and $m_{ji}^{(t)}$ is also explicitly embedded in spherical Bessel function $a_{\text{SBE}}^{(kj, ji)}$ to update $m_{kji}^{(t)}$.

We trained ETGNN with the forces of the molecular dynamics (MD) trajectories of the extended systems provided in ref 39. The extended systems consist of supercells of inorganic and organic crystals and also contain clusters, high-entropy alloys (HEAs), and two-dimensional materials. The organic polymer pyridine and bulk TiO₂ contain two and three phases, respectively, which can test the prediction accuracy of the model for different phases. HEA CoCrFeMnNi contains five metal elements, and each element is randomly arranged in the crystal, which is a great challenge to the model. DeepPot-SE⁴⁰ and DeePMID⁴¹ are two representative neural network potential energy surface (PES) models, which calculate the forces by using the gradients of the potential energy: $\vec{F}_i = -\nabla_i E$. For each subsystem, 90% randomly selected structures are used for training, and the remaining 10% are used for testing.⁴⁰ As one can see in Table 1, the RMSEs achieved by the ETGNN model are lower than those achieved by DeepPot-SE and DeePMID on nearly all of the subsystems.

Similar to the atomic forces, some higher-order tensors can be obtained by taking the first or second partial derivative of energy with respect to an external field.⁴² Here we compare the previous gradient-based tensor prediction method with that of our ETGNN models. We have successfully trained the ETGNN models on the data set of first-order dipole moment μ , second-order polarizability tensor α , and atomic second-order chemical shift tensors σ of two organic molecules (ethanol and allyl *p*-tolyl ether). The expansion formulas of the dielectric tensor and Born effective charge tensor were used to decompose the polarizability and the atomic chemical shift tensor, respectively. We compared the results of ETGNN with those of FieldSchNet,⁴² which computes these response properties using derivatives of total energies. Table 2 shows the comparison of the mean absolute errors (MAEs) of ETGNN and FieldSchNet trained on ethanol in a vacuum and allyl *p*-tolyl ether in vacuum. As one can see in Table 2, the prediction error of ETGNN for almost all of the tensor properties listed in Table 2 is much smaller than that of FieldSchNet.

SA-GPR³³ and the linear model³⁶ are two previously reported equivariant models for predicting the tensor properties of molecules. We compared the precision of SA-GPR,³³ the linear model,³⁶ and ETGNN on the magnetic anisotropy

Table 1. Comparison of the Root-Mean-Square Errors (RMSEs) of the Forces Predicted for the Extended Systems by ETGNN, DeepPot-Se, and DeePMD^a

system	subsystem	DeepPot-Se	DeePMD	ETGNN
bulk Cu	FCC solid	90	90	89
bulk Ge	diamond solid	38	35	7
bulk Si	diamond solid	36	31	5
bulk Al ₂ O ₃	trigonal solid	49	55	36
bulk C ₅ H ₅ N	pyridine-I	25	25	14
	pyridine-II	39	39	19
bulk TiO ₂	rutile	137	163	61
	anatase	181	216	82
	brookite	94	109	44
MoS ₂ and Pt	MoS ₂ slab	23	34	27
	bulk Pt	84	226	27
	Pt surface	105	187	37
	Pt cluster	201	255	68
HEA CoCrFeMnNi	Pt on MoS ₂	94	127	33
	random occupations-I	394	481	373
	random occupations-II	410	576	385

^aThe lowest RMSE among the considered models for each subsystem is displayed in bold. The values are in units of millielectron volts per angstrom.

Table 2. Comparison of the Mean Absolute Errors (MAEs) of ETGNN and FieldSchNet Trained on Ethanol in a Vacuum and Allyl *p*-Tolyl Ether in a Vacuum^a

property	units	allyl <i>p</i> -tolyl ether (vacuum)		ethanol (vacuum)	
		FieldSchNet	ETGNN	FieldSchNet	ETGNN
μ	debyes	0.003	0.00024	0.004	0.0018
α	Bohr ³	0.039	0.0202	0.008	0.025
σ_{all}	parts per million	0.273	0.0293	0.169	0.00735
σ_C	parts per million	0.301	0.0417	0.194	0.00721
σ_H	parts per million	0.045	0.0202	0.123	0.00385
σ_O	parts per million	2.732	0.0147	0.401	0.00286

^aThe lowest MAE between the two models for each property is displayed in bold.

tensor data sets³⁶ for Co(H₂O)_x and CoL₂ [H₂L = 1,2-bis(methanesulfonamido)benzene]. The Co(H₂O)_x and CoL₂ data sets consist of 600 and 150 molecular structures, respectively. Each data set is divided into training and test sets in a ratio of 0.8:0.2. Figure 3 shows the precision of these three models for the test sets. As shown in Figure 3, The RMSE of ETGNN is significantly lower than that of the other two models.

On the basis of the tensor expansion formulas, we tested the prediction accuracy of ETGNN for the BECs, the DL tensors ϵ_{∞} (electronic contribution), and the PZ tensors of crystals. The training data sets are from the density functional perturbation theory (DFPT) calculations on 3190 Al₂O₃, 3992 SiO₂, 10 000 HfO₂, 3211 AlN, 3000 CdS, and 3000 ZnO random perturbed structures. HfO₂ is a potential complementary metal oxide semiconductor (CMOS) compatible ferroelectric memory material and can form many crystal structures.^{43–46} The perturbed structures of HfO₂ consist of

5000 structures with six-coordinated Hf ions and 5000 structures with eight-coordinated Hf ions. Each model was trained with 60% of the data, validated with 20% of the data, and tested with the remaining 20% of the data. The comparisons of the DFT-calculated tensors and the ETGNN-predicted tensors on the test data sets of the perturbed structures are shown in Figure 4. As one can see in Figure 4, each component of the BECs predicted by ETGNN is very close to the corresponding component of the BECs calculated by DFT. The mean absolute errors (MAEs) of the components of the predicted BECs on the Al₂O₃, SiO₂, and HfO₂ test sets are only 1.18×10^{-2} , 4.28×10^{-3} , and 1.94×10^{-3} e, respectively. The MAEs of the components of the predicted ϵ_{∞} on the Al₂O₃, SiO₂, and HfO₂ test sets are only 5.54×10^{-3} , 1.98×10^{-3} , and 2.86×10^{-3} , respectively. For the third-order PZ tensor, ETGNN still maintains a high prediction accuracy. The MAEs of the components of the predicted PZ tensors on the AlN, CdS, and ZnO test sets are only 3.29×10^{-4} , 4.69×10^{-4} , and 5.59×10^{-4} C/m², respectively. The tensor prediction test on these perturbed structures indicates that invariant GNNs can achieve high prediction accuracy in principle by using the edge-based tensor expressions proposed in this work.

ETGNN has also been tested on the BECs of ~5000 nonmetallic materials in the JARVIS-DFT database.⁴⁷ This data set contains more than 80 elements in the periodic table. The DFT values of the structures containing some rare earth elements may have large calculation errors because the pseudopotentials are often difficult to use to accurately describe the complex electronic structures of the rare earth elements. This will affect the prediction performance of the ML methods. For the JARVIS-DFT data set, 70%, 20%, and 10% of the calculated values were used as the training, validation, and test sets, respectively. The MAE of ETGNN on the test set of BECs still reached a low value of 0.045 e. Figure 5a shows that most of the predicted values agree well with the DFT-calculated values. This high prediction accuracy means that ETGNN can be used as a universal model to calculate BECs with a speed much faster than that of DFT.

For comparison with the traditional ML models, an ETGNN model was trained for maximum BECs in the JARVIS-DFT data set. For the maximum component of the BECs, the MAE of the ETGNN model on the test set is 0.12 e, which is only one-fifth of that of the classical force-field-inspired descriptor (CFID) model used in ref 46. It was reported that large deviations between the experimental and calculated dielectric constants can be seen for approximately 20% of the compounds.⁴⁸ Thus, predicting the dielectric tensors of various crystals was thought to be a huge challenge. The ETGNN regression model for the dielectric tensors was successfully trained and achieved an MAE of 0.21 on the test data set. ETGNN automatically develops physical insights into the Born effective charge of materials while training on the JARVIS-DFT data set. Figure 5b shows that the embedded features from the ETGNN model trained for the mean diagonal value of BECs have a distinct separation for atoms with different mean diagonal values. The mean diagonal values of the data points in the principal component analysis (PCA) projection plot gradually increase from the top left to the top right. The mean diagonal values of the BECs of metal elements in oxides are positive, while the mean diagonal values of some group VIII metal elements such as Ru, Fe, and Co in multielement alloys have negative minima. The mean diagonal values of

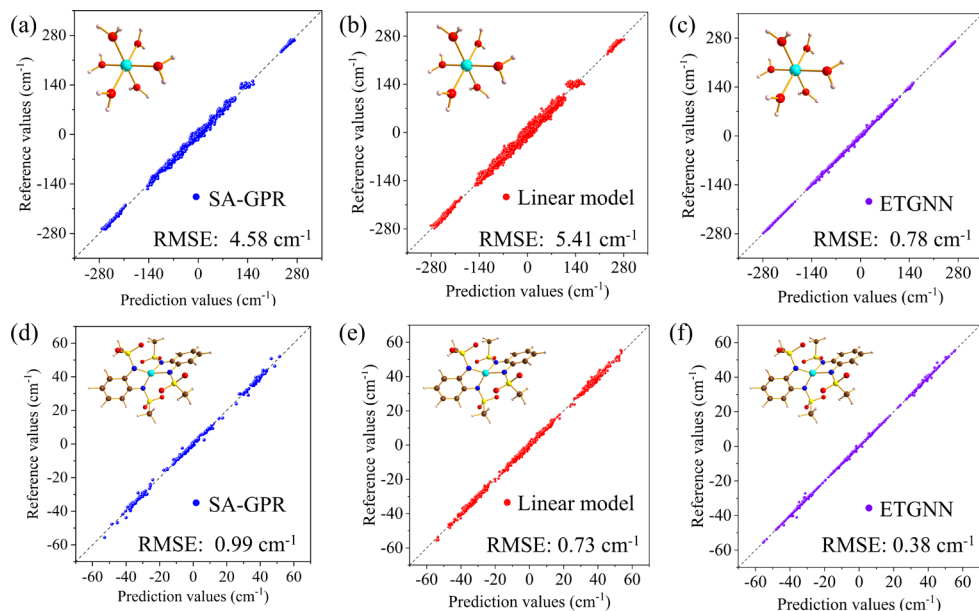


Figure 3. Learning of magnetic anisotropy with SA-GPR, the linear model, and ETGNN. Comparison of the predicted magnetic anisotropy tensors for $\text{Co}(\text{H}_2\text{O})_x$ using (a) SA-GPR, (b) the linear model, and (c) ETGNN with reference values. Comparison of the predicted magnetic anisotropy tensors for CoL_2 using (d) SA-GPR, (e) the linear model, and (f) ETGNN with reference values.

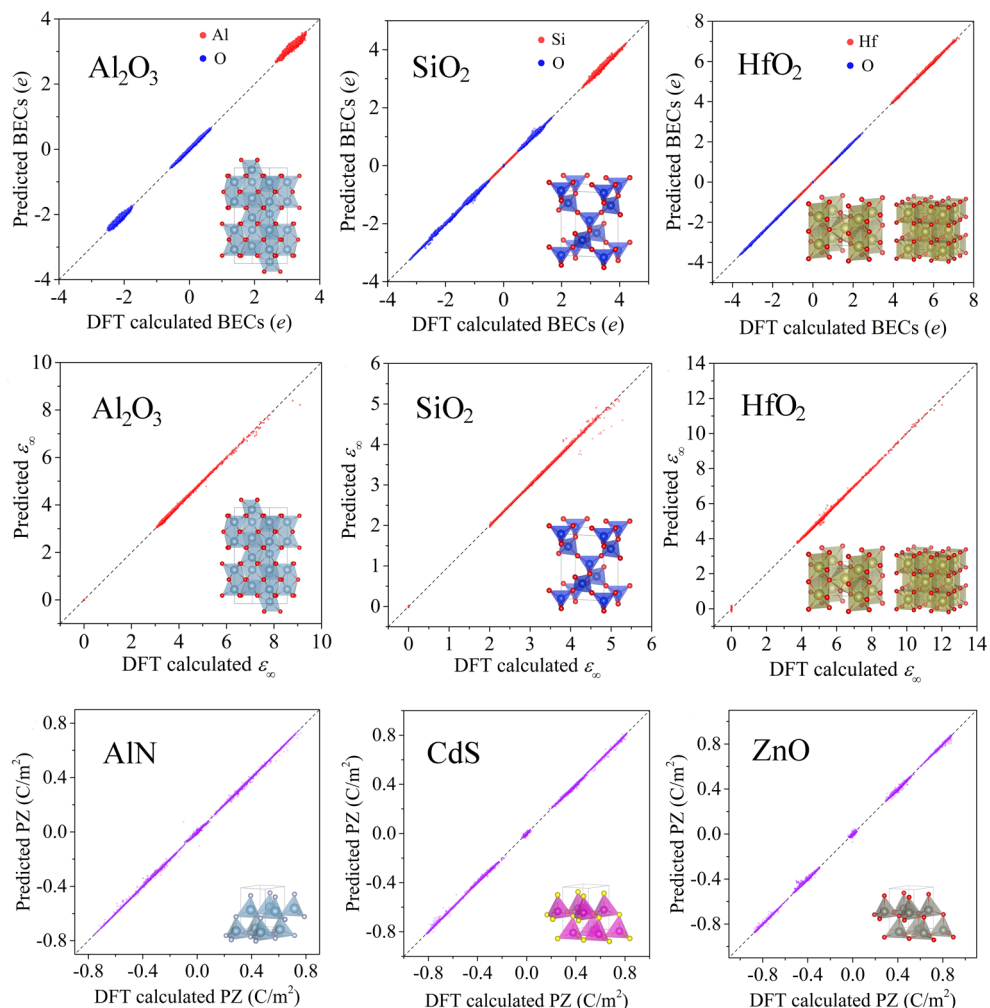


Figure 4. Comparison of ETGNN-predicted values and DFT-calculated values on the BECs and DL and PZ tensors of the testing perturbed structure data set.

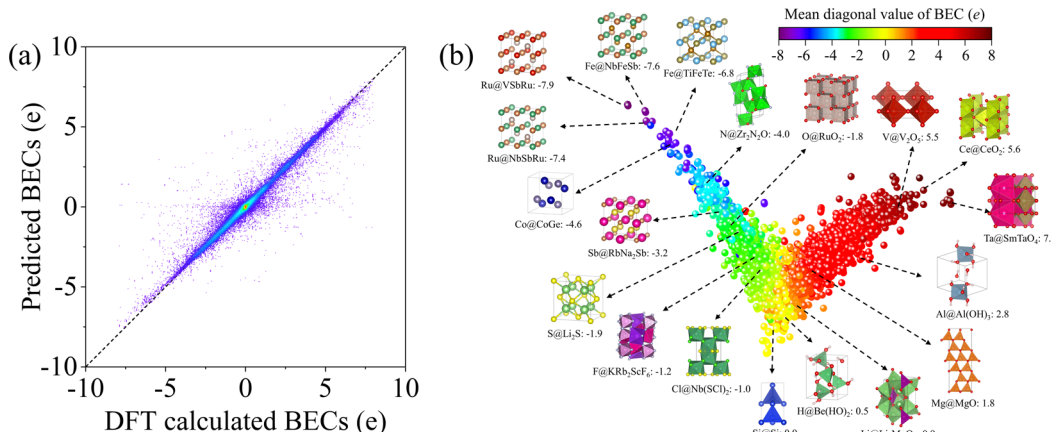


Figure 5. Prediction results on the JARVIS-DFT data set. (a) Comparison of the predicted and calculated Born effective charges on the JARVIS-DFT data set. (b) Visualizing the embedding space of the atoms in the JARVIS-DFT data set using PCA. Each point on the graph is colored according to the mean diagonal value of the BEC of each atom.

group VA, VIA, and VIIA nonmetallic elements increase sequentially. The BECs of atoms in some single-element crystals, such as Si and He, are almost zero, lying on the border between positive and negative BECs in the PCA projection plot. The mean diagonal values of hydrogen, alkali, group IIA, and group IIIA metal elements are positive and increase sequentially. Some transition metal cations have mean diagonal values of BECs larger than those of other elements and are located in the region closer to the top right corner. The representation learned by ETGNN can be used to characterize and understand the large chemical spaces of the BECs of the materials.

In conclusion, we generalized the atom-centric framework of GNNs to tensors and proposed a general tensor prediction framework that decomposes the tensorial properties by local spatial components projected on the edge directions of clusters with varying sizes. On the basis of this idea, we have given the explicit formula of the body-ordered expansions of general tensors. These expansions are rotationally equivalent, while the coefficients in the expansions are invariant and can be predicted by various traditional invariant GNNs. We designed an ETGNN based on an invariant GNN to verify our tensor prediction framework. The precision of ETGNN outperforms the state-of-the-art models for a variety of tensor prediction tasks. For the force prediction on the extended systems, ETGNN outperforms DeePMD and DeepPot-SE on nearly all of the test systems. This shows that the tensor prediction framework can also be used for the precise potential fields of various molecules and crystals. For the response properties, including first-order dipole moment μ , second-order polarizability tensor α , and atomic second-order chemical shift tensors σ , the accuracy achieved by ETGNN is much higher than that of FieldSchNet, which predicts these tensors by the back forward of the gradients. This shows that ETGNN has a strong fitting ability for the response properties of various external fields. ETGNN was also used to predict the BECs and DL and PZ tensors of the random perturbed structures and achieved a very high accuracy. The evaluation of ETGNN on these perturbed structures indicates that the tensor expansions proposed in this work are valid and general. In addition, we have successfully trained the regression models of ETGNN to predict the BECs of ~5000 nonmetallic materials containing more than 80 elements. The previous work could not handle

the tensors and successfully trained the regression models only for the maximum component of the tensors.⁴⁷ Taking into account the errors of the tensors calculated by DFPT, we found the mean absolute error of the predicted tensors in this data set is relatively low. Our study suggests that ETGNN is a general, efficient, and accurate framework for GNNs to predict tensorial properties.

ASSOCIATED CONTENT

Supporting Information

The Supporting Information is available free of charge at <https://pubs.acs.org/doi/10.1021/acs.jpcllett.3c01200>.

Supplementary discussions and training details ([PDF](#))

AUTHOR INFORMATION

Corresponding Author

Hongjun Xiang — Key Laboratory of Computational Physical Sciences (Ministry of Education), Institute of Computational Physical Sciences, State Key Laboratory of Surface Physics, and Department of Physics, Fudan University, Shanghai 200433, China; Shanghai Qi Zhi Institute, Shanghai 200030, China; Collaborative Innovation Center of Advanced Microstructures, Nanjing 210093, China; orcid.org/0000-0002-9396-3214; Email: hxiang@fudan.edu.cn

Authors

Yang Zhong — Key Laboratory of Computational Physical Sciences (Ministry of Education), Institute of Computational Physical Sciences, State Key Laboratory of Surface Physics, and Department of Physics, Fudan University, Shanghai 200433, China; Shanghai Qi Zhi Institute, Shanghai 200030, China

Hongyu Yu — Key Laboratory of Computational Physical Sciences (Ministry of Education), Institute of Computational Physical Sciences, State Key Laboratory of Surface Physics, and Department of Physics, Fudan University, Shanghai 200433, China; Shanghai Qi Zhi Institute, Shanghai 200030, China

Xingao Gong — Key Laboratory of Computational Physical Sciences (Ministry of Education), Institute of Computational Physical Sciences, State Key Laboratory of Surface Physics, and Department of Physics, Fudan University, Shanghai 200433, China

200433, China; Shanghai Qi Zhi Institute, Shanghai 200030, China; Collaborative Innovation Center of Advanced Microstructures, Nanjing 210093, China

Complete contact information is available at:
<https://pubs.acs.org/10.1021/acs.jpcllett.3c01200>

Author Contributions

[†]Y.Z. and H.Y. contributed equally to this work.

Notes

The authors declare no competing financial interest.

ACKNOWLEDGMENTS

This work is supported by NSFC (Grants 811825403, 11991061, and 12188101) and the Guangdong Major Project of Basic and Applied Basic Research [Future functional materials under extreme conditions (2021B0301030005)].

REFERENCES

- (1) Butler, K. T.; Davies, D. W.; Cartwright, H.; Isayev, O.; Walsh, A. Machine learning for molecular and materials science. *Nat. 2018*, **559**, 547–555.
- (2) Pollice, R.; Dos Passos Gomes, G.; Aldeghi, M.; Hickman, R. J.; Krenn, M.; Lavigne, C.; Lindner-D'Addario, M.; Nigam, A.; Ser, C. T.; Yao, Z.; Aspuru-Guzik, A. Data-driven strategies for accelerated materials design. *Acc. Chem. Res.* **2021**, *54*, 849–860.
- (3) Morgan, D.; Jacobs, R. Opportunities and challenges for machine learning in materials science. *Annu. Rev. Mater. Res.* **2020**, *50*, 71–103.
- (4) Hart, G. L. W.; Mueller, T.; Toher, C.; Curtarolo, S. Machine learning for alloys. *Nat. Rev. Mater.* **2021**, *6*, 730–755.
- (5) Lu, S. H.; Zhou, Q. H.; Ouyang, Y. X.; Guo, Y. L.; Li, Q.; Wang, J. L. Accelerated discovery of stable lead-free hybrid organic-inorganic perovskites via machine learning. *Nat. Commun.* **2018**, *9*, 3405.
- (6) Cai, X.; Zhang, Y.; Shi, Z.; Chen, Y.; Xia, Y.; Yu, A.; Xu, Y.; Xie, F.; Shao, H.; Zhu, H.; Fu, D.; Zhan, Y.; Zhang, H. Discovery of lead-free perovskites for high-performance solar cells via machine learning: ultrabroadband absorption, low radiative combination, and enhanced thermal conductivities. *Adv. Sci.* **2022**, *9*, 2103648.
- (7) Kitchin, J. R. Machine learning in catalysis. *Nat. Catal.* **2018**, *1*, 230–232.
- (8) Ma, S. C.; Liu, Z. P. Machine learning for atomic simulation and activity prediction in heterogeneous catalysis: current status and future. *ACS. Catal.* **2020**, *10*, 13213–13226.
- (9) Zhang, N.; Yang, B. P.; Liu, K.; Li, H. M.; Chen, G.; Qiu, X. Q.; Li, W. Z.; Hu, J. H.; Fu, J. W.; Jiang, Y.; Liu, M.; Ye, J. H. Machine learning in screening high performance electrocatalysts for CO₂ reduction. *Small Methods* **2021**, *5*, 2100987.
- (10) Liu, Y. T.; Zhou, Q.; Cui, G. L. Machine learning boosting the development of advanced lithium batteries. *Small Methods* **2021**, *5*, 2100442.
- (11) Lv, C. D.; Zhou, X.; Zhong, L. X.; Yan, C. S.; Srinivasan, M.; Seh, Z. W.; Liu, C. T.; Pan, H. G.; Li, S. Z.; Wen, Y. G.; Yan, Q. Y. Machine learning: an advanced platform for materials development and state prediction in lithium-ion batteries. *Adv. Mater.* **2022**, *34*, 2101474.
- (12) Wang, T.; Zhang, C.; Snoussi, H.; Zhang, G. Machine learning approaches for thermoelectric materials research. *Adv. Funct. Mater.* **2020**, *30*, 1906041.
- (13) Chmiela, S.; Tkatchenko, A.; Sauceda, H. E.; Poltavsky, I.; Schutt, K. T.; Muller, K. R. Machine learning of accurate energy-conserving molecular force fields. *Sci. Adv.* **2017**, *3*, 1603015.
- (14) Fonseca, G.; Poltavsky, I.; Vassilev-Galindo, V.; Tkatchenko, A. Improving molecular force fields across configurational space by combining supervised and unsupervised machine learning. *J. Chem. Phys.* **2021**, *154*, 124102.
- (15) Vassilev-Galindo, V.; Fonseca, G.; Poltavsky, I.; Tkatchenko, A. Challenges for machine learning force fields in reproducing potential energy surfaces of flexible molecules. *J. Chem. Phys.* **2021**, *154*, No. 094119.
- (16) Cheng, Z.; Du, J. H.; Zhang, L.; Ma, J.; Li, W.; Li, S. H. Building quantum mechanics quality force fields of proteins with the generalized energy-based fragmentation approach and machine learning. *Phys. Chem. Chem. Phys.* **2022**, *24*, 1326–1337.
- (17) Schutt, K. T.; Arbabzadah, F.; Chmiela, S.; Muller, K. R.; Tkatchenko, A. Quantum-chemical insights from deep tensor neural networks. *Nat. Commun.* **2017**, *8*, 13890.
- (18) Schutt, K. T.; Sauceda, H. E.; Kindermans, P. J.; Tkatchenko, A.; Muller, K. R. SchNet - A deep learning architecture for molecules and materials. *J. Chem. Phys.* **2018**, *148*, 241722.
- (19) Xie, T.; Grossman, J. C. Crystal graph convolutional neural networks for an accurate and interpretable prediction of material properties. *Phys. Rev. Lett.* **2018**, *120*, 145301.
- (20) Unke, O. T.; Meuwly, M. PhysNet: A neural network for predicting energies, forces, dipole moments, and partial charges. *J. Chem. Theory Comput.* **2019**, *15*, 3678–3693.
- (21) Park, C. W.; Wolverton, C. Developing an improved crystal graph convolutional neural network framework for accelerated materials discovery. *Phys. Rev. Mater.* **2020**, *4*, No. 063801.
- (22) Gasteiger, J.; Groß, J.; Günemann, S. Directional message passing for molecular graphs. *arXiv* **2020**, DOI: [10.48550/arXiv.2003.03123](https://doi.org/10.48550/arXiv.2003.03123).
- (23) Haghhighatlari, M.; Li, J.; Heidar-Zadeh, F.; Liu, Y.; Guan, X.; Head-Gordon, T. Learning to make chemical predictions: the interplay of feature representation, data, and machine learning algorithms. *Chem.* **2020**, *6*, 1527–1542.
- (24) Unke, O. T.; Meuwly, M. A reactive, scalable, and transferable model for molecular energies from a neural network approach based on local information. *J. Chem. Phys.* **2018**, *148*, 241708.
- (25) Faber, F. A.; Christensen, A. S.; Huang, B.; von Lilienfeld, O. A. Alchemical and structural distribution based representation for universal quantum machine learning. *J. Chem. Phys.* **2018**, *148*, 241717.
- (26) Bartok, A. P.; Kondor, R.; Csanyi, G. On representing chemical environments. *Phys. Rev. B* **2013**, *87*, 184115.
- (27) Thomas, N.; Smidt, T.; Kearnes, S.; Yang, L.; Li, L.; Kohlhoff, K.; Riley, P. Tensor field networks: rotation- and translation-equivariant neural networks for 3D point clouds. *arXiv* **2018**, DOI: [10.48550/arXiv.1802.08219](https://doi.org/10.48550/arXiv.1802.08219).
- (28) Weiler, M.; Geiger, M.; Welling, M.; Boomsma, W.; Cohen, T. 3D steerable CNNs: learning rotationally equivariant features in volumetric data. *arXiv* **2018**, DOI: [10.48550/arXiv.1807.02547](https://doi.org/10.48550/arXiv.1807.02547).
- (29) Brandstetter, J.; Hessellink, R.; van der Pol, E.; Bekkers, E.; Welling, M. Geometric and physical quantities improve E(3)-equivariant message passing. *arXiv* **2021**, DOI: [10.48550/arXiv.2110.02905](https://doi.org/10.48550/arXiv.2110.02905).
- (30) Batzner, S.; Musaelian, A.; Sun, L. X.; Geiger, M.; Mailoa, J. P.; Kornbluth, M.; Molinari, N.; Smidt, T. E.; Kozinsky, B. E(3)-equivariant graph neural networks for data-efficient and accurate interatomic potentials. *Nat. Commun.* **2022**, *13*, 2453.
- (31) Batatia, I.; Batzner, S.; Kovacs, D. a. P. e.; Musaelian, A.; Simm, G. N. C.; Drautz, R.; Ortner, C.; Kozinsky, B.; Csányi, G. The design space of E(3)-equivariant atom-centered interatomic potentials. *arXiv* **2022**, DOI: [10.48550/arXiv.2205.06643](https://doi.org/10.48550/arXiv.2205.06643).
- (32) Musaelian, A.; Batzner, S.; Johansson, A.; Sun, L.; Owen, C. J.; Kornbluth, M.; Kozinsky, B. Learning local equivariant representations for large-scale atomistic dynamics. *Nat. Commun.* **2023**, *14*, 579.
- (33) Grisafi, A.; Wilkins, D. M.; Csanyi, G.; Ceriotti, M. Symmetry-adapted machine learning for tensorial properties of atomistic systems. *Phys. Rev. Lett.* **2018**, *120*, No. 036002.
- (34) Glick, Z. L.; Koutsoukas, A.; Cheney, D. L.; Sherrill, C. D. Cartesian message passing neural networks for directional properties: fast and transferable atomic multipoles. *J. Chem. Phys.* **2021**, *154*, 224103.
- (35) Zaverkin, V.; Netz, J.; Zills, F.; Kohn, A.; Kastner, J. Thermally averaged magnetic anisotropy tensors via machine learning based on Gaussian moments. *J. Chem. Theory Comput.* **2022**, *18*, 1–12.

- (36) Nguyen, V. H. A.; Lunghi, A. Predicting tensorial molecular properties with equivariant machine learning models. *Phys. Rev. B* **2022**, *105*, 165131.
- (37) Behler, J.; Parrinello, M. Generalized neural-network representation of high-dimensional potential-energy surfaces. *Phys. Rev. Lett.* **2007**, *98*, 146401.
- (38) Gasteiger, J.; Giri, S.; Margraf, J. T.; Günnemann, S. Fast and uncertainty-aware directional message passing for non-equilibrium molecules. *arXiv* **2020**, DOI: 10.48550/arXiv.2011.14115.
- (39) Clevert, D.-A.; Unterthiner, T.; Hochreiter, S. Fast and accurate deep network learning by exponential linear units (ELUs). *arXiv* **2015**, DOI: 10.48550/arXiv.1511.07289.
- (40) Zhang, L. F.; Han, J. Q.; Wang, H.; Saidi, W. A.; Car, R.; E, W. N. End-to-end symmetry preserving inter-atomic potential energy model for finite and extended systems. *Adv. Neur. In.* **2018**, *31*, 4441–4451.
- (41) Wang, H.; Zhang, L. F.; Han, J. Q.; E, W. N. DeePMD-kit: A deep learning package for many-body potential energy representation and molecular dynamics. *Comput. Phys. Commun.* **2018**, *228*, 178–184.
- (42) Gastegger, M.; Schutt, K. T.; Muller, K. R. Machine learning of solvent effects on molecular spectra and reactions. *Chem. Sci.* **2021**, *12*, 11473–11483.
- (43) Park, M. H.; Lee, Y. H.; Mikolajick, T.; Schroeder, U.; Hwang, C. S. Review and perspective on ferroelectric HfO₂-based thin films for memory applications. *Mrs Commun.* **2018**, *8*, 795–808.
- (44) Gutowski, M.; Jaffe, J. E.; Liu, C. L.; Stoker, M.; Hegde, R. I.; Rai, R. S.; Tobin, P. J. Thermodynamic stability of high-K dielectric metal oxides ZrO₂ and HfO₂ in contact with Si and SiO₂. *Appl. Phys. Lett.* **2002**, *80*, 1897–1899.
- (45) Boescke, T. S.; Muller, J.; Brauhaus, D.; Schroder, U.; Bottger, U. Ferroelectricity in hafnium oxide thin films. *Appl. Phys. Lett.* **2011**, *99*, 102903.
- (46) Pesic, M.; Kunzeth, C.; Hoffmann, M.; Mulaosmanovic, H.; Muller, S.; Breyer, E. T.; Schroeder, U.; Kersch, A.; Mikolajick, T.; Slesazeck, S. A computational study of hafnia-based ferroelectric memories: from ab initio via physical modeling to circuit models of ferroelectric device. *J. Comput. Electron.* **2017**, *16*, 1236–1256.
- (47) Choudhary, K.; Garrity, K. F.; Sharma, V.; Biacchi, A. J.; Hight Walker, A. R.; Tavazza, F. High-throughput density functional perturbation theory and machine learning predictions of infrared, piezoelectric, and dielectric responses. *npj Comput. Mater.* **2020**, *6*, 64.
- (48) Umeda, Y.; Hayashi, H.; Moriwake, H.; Tanaka, I. Prediction of dielectric constants using a combination of first principles calculations and machine learning. *Jpn. J. Appl. Phys.* **2019**, *58*, SLLC01.